Optical pump-and-probe test system for thermal characterization of thin metal and phase-change films

Kazuo Watabe, Pavel Polynkin, and Masud Mansuripur

A single-shot optical pump-and-probe test system is reported. The system is designed for thermal characterization of thin-film samples that can change their phase state under the influence of a short and intense laser pulse on a subnanosecond time scale. In combination with numerical analysis, the system can be used to estimate thermal constants of thin films, such as specific heat and thermal conductivity. In-plane and out-of plane thermal conductivity can be estimated independently. The system is intended for use in research on optical data storage and material processing with pulsed laser light. The system design issues are discussed. As application examples, we report on using the system to study thermal dynamics in two different thin-film samples: a gold film on a glass substrate (a single-phase system) and the quadrilayer phase-change stack typical in optical data-storage applications.

OCIS codes: 120.4820, 120.6810, 210.4590, 240.0310, 310.6870.

1. Introduction

Current research on ultrafast thermal dynamics in material surfaces and composite multilayer thin films is motivated in part by recent advances in such areas of applied science as material processing with pulsed laser light[1] and optical data storage.[2] Various thermoreflectance techniques have been used as an effective noncontact tool to study thin films. Typically, the sample is locally heated by a short pulse of laser light. If the reflection coefficient of the sample is known as a function of temperature, then monitoring the reflection from the heated surface gives insight into the heat flow within the sample.

All thermoreflectance methods can be loosely divided into two broad classes. With setups of the first type[3–6] the so-called pump-and-probe technique is used with phase-sensitive detection of the reflectivity change caused by the chopped pump beam from a mode-locked laser. These systems are fast and accurate in terms of resolving small changes in the sample reflectivity. However, they cannot be used to study phase-change media because in normal operation the sample is supposed to recover its original state within the time interval between successive laser pulses (typically a few nanoseconds).

Systems of the second kind[7,8] use a pulsed pump laser and a separate weak cw probe light source. A single pump pulse hits the sample and at the same time triggers a photodetector that reads the intensity of the cw probe light beam reflected from the heated sample surface. The detector then produces a time-dependent output trace that is proportional to the instantaneous reflectivity from the sample. Systems of this kind are quite easy to operate as there is no delay line to be adjusted for either the pump or the probe beams. In addition, these systems can be used to study the phase-change media. However, their time resolution is typically of the order of tens of nanoseconds or more, which can be inadequate to study fast phase-change processes such as amorphization in optical data-storage disks.

In addition to the two classes of systems described above, there are several reports on quite sophisticated and costly approaches that yield both high sensitivity and good time resolution.[9–12] These systems are not straightforward to operate and might not be suitable for extensive and routine sample testing.

In this paper we report on a new thermoreflectance test system that allows for thermal characterization of phase-change thin-film and surface samples on a subnanosecond time scale. Our system is based on

The authors are with the Optical Sciences Center, University of Arizona, 1630 East University Boulevard, Tucson, Arizona 85721. K. Watabe is on leave from the Core Technology Center, Toshiba Corporation, 8 Shinsugita-cho, Isogo-ku, Yokohama 235-8522, Japan. The e-mail address for P. Polynkin is ppolynkin@optics.arizona.edu.

Received 4 March 2004; revised manuscript received 7 January 2005; accepted 20 January 2005.

0003-6935/05/163167-07$15.00/0

the pump-and-probe approach with detection of individual probe pulses. To combat the measurement noise, the coherence function of the pump laser was modified by use of nonlinear properties of a single-mode optical fiber. The time resolution and sensitivity to the reflectivity change for our system are estimated as ~0.5 ns and 0.1%, respectively. The system is capable of providing information about both in-plane and out-of-plane thermal constants of thin-film and surface samples. As application examples, two different types of thin-film sample were studied with our approach. The first sample was a 65-nm-thick gold film on a glass substrate (a single-phase system). By comparing the experimental data with the results of numerical modeling, we were able to determine that the gold film's specific heat was close to that of bulk gold, whereas its thermal conductivity was approximately one half of the bulk value. Note here that since this thin-film sample is a single-phase system, the lock-in detection-based approach would yield better results as it is typically more sensitive. Our reason for choosing this particular sample was motivated by the desire to show the ultimate sensitivity of our system. The second sample was a quadrilayer film deposited on a polycarbonate substrate. Thin films of this kind are common in optical data-storage applications, as they can exist in two stable phase states, polycrystalline and amorphous, and the reversible phase transitions between the two states can be initiated by the localized heating caused by short, focused laser pulses. Using our system, we found that the heat-induced amorphization of the sample occurs on a time scale shorter than ~1 ns. In addition, we found the energy of the laser pulse that is needed to create the amorphous mark on the sample, as well as the pulse energy that causes the permanent sample burnout.

This paper is organized as follows. In Section 2 we describe the system and comment on several design issues that are important to decrease the measurement noise. In Section 3 we report on using our system to estimate thermal constants of a thin gold film on a glass substrate and to study the dynamics of the phase transition in the quadrilayer thin-film medium commonly used in optical data storage. Concluding remarks are given in Section 4.

2. Experimental Setup

Our system intended for the study of thermal dynamics of phase transitions in thin films and surfaces is based on the pump-and-probe approach. The choice of particular components of the system was motivated by specifics of the application. The system is schematically shown in Fig. 1 and operates as follows.

An intracavity frequency-doubled, passively Q-switched solid-state laser (JDS Uniphase Nanolaser product) generates a train of linearly polarized, ~600-ps-long pulses with a repetition rate of 5.7 kHz. The laser wavelength is 532 nm. Directly at the output of the laser, the total energy of each pulse is ≈4.5 μJ and is randomly fluctuating from one pulse to another by ~2.5% (peak to peak). The output

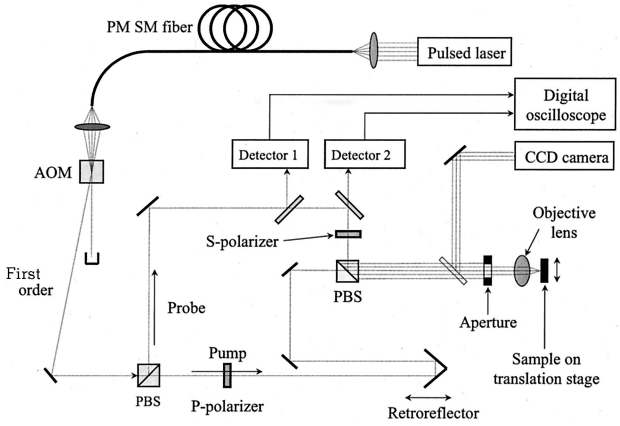

Fig. 1. Schematic of the pump-and-probe test system. PM SM, polarization-maintaining single-mode; AOM, acousto-optic modulator.

laser light is sent through a few meters-long single-mode optical fiber that serves the dual purposes of spatially filtering the beam and reducing the coherent pump–probe cross talk, as we elaborate on in Section 3. Upon exiting the fiber, the light is focused onto an acousto-optic (AO) beam deflector driven by an electrical ac signal. The frequency of the AO driver determines the angular separation between the zeroth- and the first-order deflected beams and is kept unchanged at 440 MHz, yielding a constant separation of ≈ 3 deg between the two beams. The first-order diffracted beam is used as a light source in our system, and the zeroth-order beam is blocked. In experiments with phase-change media, the optical energy has to be delivered to the sample one pulse at a time. Accordingly, the ac driver of the AO crystal is modulated by single, 200-μs-long square pulses. Thus the crystal acts as an optical gate, as only a single pulse from the laser falls inside that 200-μs-long window. In addition, the amplitude of the AO driver waveform determines the fraction of the light intensity deflected into the first-order beam, which is used to adjust the total energy of the pulses. The first diffraction order output of the AO deflector is collimated and split into two light beams by means of a polarizing beam splitter (PBS). The linear polarization of light entering the PBS is tuned so that the two orthogonally polarized beams at the sample have intensities that differ by a factor of 40, with the stronger beam being the pump and the weaker one the probe. The two beams then follow the standard pump-and-probe arrangement. Their polarizations are kept orthogonal to one another all the way throughout the optical path. The beams, after they are delayed with respect to one another by means of a variable delay line for the pump, are recombined at another PBS, before they are focused onto the sample. Depending on the numerical aperture (NA) of the objective lens used, the $1/e$ intensity diameter of the focused light spot for both beams in the sample plane can be varied, in our case between ~1 and ~15 μm. Data taken with different spot sizes can be used to

extract information about in-plane and out-of-plane thermal properties of the sample. Upon reflection from the sample, the probe is once again separated from the pump and directed to a photodetector shown as detector 2 in Fig. 1. The detector has a high slew rate and a bandwidth of 50 MHz, which is much narrower than the inverse duration of the pulse; therefore the peak value of the detected electrical waveform is proportional to the energy of the probe beam reflected from the sample, a direct measure of the instantaneous reflectivity of the sample. Our system allows for the delay between pump and probe pulses to be varied in the range from -5 to $+15$, with an accuracy of $\sim$0.3 ps that is determined solely by the translation stage used in the delay line. After each pulse, the sample is advanced by a few micrometers with the translation stage driven by a remotely controlled actuator (New Focus Picomotor product), so that, if a phase change occurs in the sample after irradiation by a single pump pulse, subsequent measurements would not be affected.

The heat-induced reflectivity change ranges from a fraction of a percent to several tens of percents. Accordingly, 0.1% was targeted as an acceptable resolution for measurement of the absolute reflectivity with our system. The most important sources of measurement error include energy fluctuations of the individual laser pulses, coherent cross talk between pump and probe beams on the photodetector, nonuniformity of the sample, and the sampling error of the data-acquisition system (i.e., digitization noise of the sampling oscilloscope). In addition, for proper modeling of the experiment, the focused spot shape and size in the sample plane have to be known, and the pump and probe beams must overlap nearly perfectly on the sample.

To help maintain the diffraction-limited beam delivery throughout the system, the (spatially) multimode output light from the laser was filtered by a few meters of a single-mode optical fiber. We monitored the placement of the sample in the focal plane of the objective lens, as well as the overlap between pump and probe beams at the sample, by observing the sample surface directly with a CCD camera. Using the camera, we also measured the focused spot size by focusing the light on a microruler placed in the sample plane and measuring the distance between zeros of the Airy pattern. To make the Airy pattern visible, the beam was slightly apertured in front of the objective lens.

To minimize the uncertainty caused by energy fluctuations of individual laser pulses, a power normalization scheme was implemented. We did this by splitting off a small fraction of the probe beam and measuring it with a separate photodetector, shown as detector 1 in Fig. 1.

In the system, the probe pulse is separated from the pump according to polarization. Since no PBS is perfect, a small fraction of the pump light will inevitably reach the detector, where it can coherently interfere with the probe light. Assume that the temporal shape of the pulses is Gaussian with a full $1/e$ intensity width τ, the pulses are delayed with respect to one another by a time interval T, and the fraction of the pump pulse reaching the detector is ξ. Then it can be shown that, if the time delay T randomly fluctuates on a scale of the optical period (which is unavoidable because of mechanical vibrations or air movement), the relative peak-to-peak uncertainty for detection of a single probe pulse is approximately given by

$$(\delta\ \text{signal})/\text{signal} \approx 2\left(\xi\,\frac{\epsilon_{\text{pump}}}{\epsilon_{\text{probe}}}\right)^{1/2}\gamma(T) = 2\left(\xi\,\frac{\epsilon_{\text{pump}}}{\epsilon_{\text{probe}}}\right)^{1/2}\exp[-(T/\tau)^2], \quad (1)$$

where $\gamma(T)$ is the autocorrelation function of the laser pulse and ϵ_{pump} and ϵ_{probe} are the total initial energies of the pump and probe pulses, respectively. The full pulse width in our setup is $\sim$600 ps; therefore it is evident from approximation (1) that the measurement uncertainty due to the coherent cross talk is at its most severe within a time delay window of $+600$ ps, which may include interesting thermal dynamics for some samples. Furthermore, since the pump beam is $\sim$40 times stronger than the probe, to suppress the relative interference noise to below 0.1% for all delays, one has to achieve better than -75-dB isolation of the pump light at the detector surface, which is nearly impossible with free-space polarizing optics. To mitigate this problem, two additional crossed polarizers were used in the optical path for the pump, which attenuated the unwanted pump beam at the detector by $\sim$40 dB. In addition, the optical fiber used to spatially filter the output beam of the laser introduced a frequency chirp in the laser pulses through the nonlinear Kerr effect in the fiber's glass. The chirp reduced the width of the autocorrelation function of the laser pulse from $\sim$500 ps to below 50 ps, confining the interval of substantial cross-talk-induced noise to below $\pm$50 ps. In Fig. 2 the measured autocorrelation function of the laser,

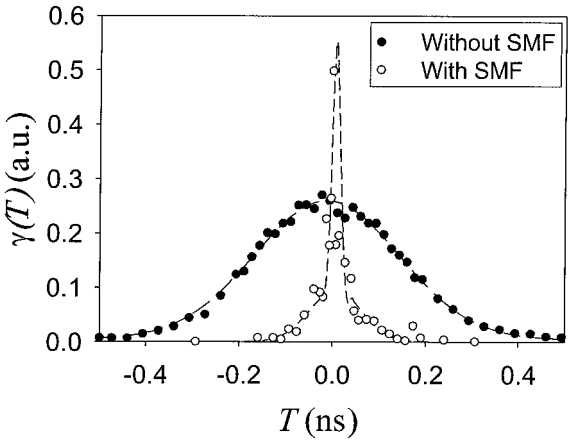

Fig. 2. Autocorrelation function of the laser pulse with and without spatial filtering with a single-mode optical fiber (SMF). Circles represent data points; curves are drawn to fit the data.

$\gamma(T)$, is shown before and after filtering by the fiber. Note here that the length of the fiber used in the experiment (~2 m) was too short to cause any substantial dispersive broadening of the laser pulses.

We estimate the absolute accuracy of our system in the reflectivity measurement with a single pulse to be below 0.5%, which is somewhat higher than our target of 0.1%. We believe that this residual uncertainty is due to the digitization error of the sampling oscilloscope used to store the output waveforms from the detectors, as well as the nonuniformity of our test samples. To further improve the accuracy, several measurements can be taken for each value of the delay between the pump and the probe pulses, but at different locations on the sample, followed by averaging the outcomes. We found that the uncertainty in the reflectivity measurements can indeed be brought down to 65 nm when we average the results of between 20 and 50 measurements obtained with individual pulses.

3. Application Examples

A. Thermal Response of a Gold Film on a Glass Substrate

As a first application example, we used our system to study thermal transport in a protected gold mirror sample. The mirror was composed of a 65-nm-thick gold layer on a float glass substrate, with a 275-nm-thick protective layer of silica. There was a thin (~5–10-nm) adhesion layer of chromium between the gold film and the substrate. Thermal properties of thin metal films are interesting because they can be quite different from those of the same material in bulk form.[7–15] However, our choice of the sample was motivated not by a desire to study these interesting properties, but to show how our system can be used to extract information about thermal constants of thin films. We also note up front that the standard pump-and-probe thermoreflectance approach based on the lock-in signal detection with a chopped pump beam would be more suitable for the study of this particular single-phase sample.

Using our system, we measured the reflectivity change of the gold mirror, as a function of the time delay between the pump and probe pulses. Three different objective lenses were used, with an effective NA of the lens–aperture system being 0.10, 0.18, and 0.36. The measured $1/e$ intensity diameter of the focused spot on the mirror surface in these cases was 3.4, 1.8, and 0.9 μm, respectively, which is close to the diffraction limit for the corresponding values of the NA. The combined data are shown in Fig. 3. Each data point results from our averaging the outcomes of 20 independent measurements with single laser pulses. The data were scaled so that the peak reflectivity change is unity in all three cases. Assuming that the reflectivity of the sample is a linear function of temperature, the curves represent normalized surface temperature, space averaged over the intensity profile of the focused probe beam in the sample plane and time averaged over the duration of the probe pulse. The latter sets a natural limit on the time resolution for our system, because any change in the reflectivity that occurs on a time scale shorter than the duration of the pulse (~600 ps) will be smeared out. The reflectivity of gold for green light (a wavelength of 532 nm) decreases with temperature[16]; therefore the curves in Fig. 3 are normalized and inverted replicas of the actual reflectivity drop versus time delay.

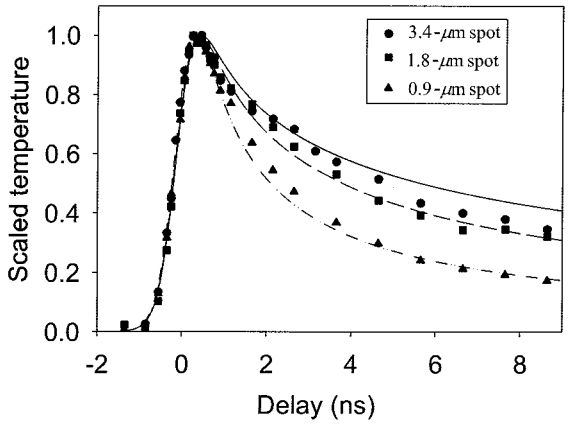

Fig. 3. Scaled temperature of the sample for three different sizes of the focused spot. Experimental data are shown with symbols; the curves represent results of thermal modeling. The parameters used in the calculations are listed in Table 1.

To fit the data, we solved (numerically) the heat diffusion equation for the system, as described in Ref. 17. In the simulations, all parameters of the system were assumed to be independent of temperature. The calculated temperature distribution in the sample plane was averaged over the spatial and temporal extent of the probe pulse and normalized. Since thermal transport in a metal layer in the direction perpendicular to the film surface occurs on a time scale too short to be detected with our system, in the modeling we did not use separate values for the in-plane and out-of plane thermal conductivity for the various sample layers. We found the best agreement between calculations and experiments with the values of thermal constants summarized in Table 1. In short, the best-fit thermal constants are the same as those for the bulk materials, except for the thermal conductivity of the gold layer, which is estimated to be approximately one half of the bulk value. The chromium adhesion layer turned out to produce no noticeable effect and was included in the simulation for completeness. The resulting curves are shown in Fig. 3

Table 1. Material Constants Used in the Numerical Simulations[a]

Material	$(n + ik)$	$c[(J/cm^3)/°C]$	$\kappa[(W/cm)/°C]$
Gold	$(0.38 + i \times 2.60)$	2.5	1.5
Chromium	$(3.19 + i \times 2.26)$	3.5	0.5
Silica	$(1.45 + i \times 0.00)$	1.6	0.014
Float glass	$(2.00 + i \times 0.012)$	2.0	0.015

[a]Complex refractive index $(n + ik)$, specific heat (c), and thermal conductivity (κ).

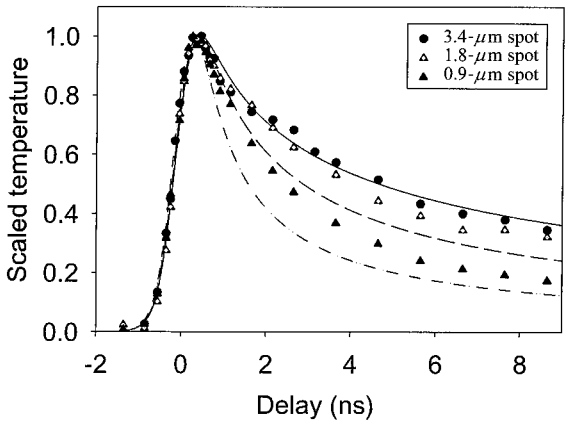

Fig. 4. Curves represent scaled temperature of the sample calculated with bulk values for all parameters of the sample for three different values of the focused spot size. Symbols represent the same experimental data as shown in Fig. 3.

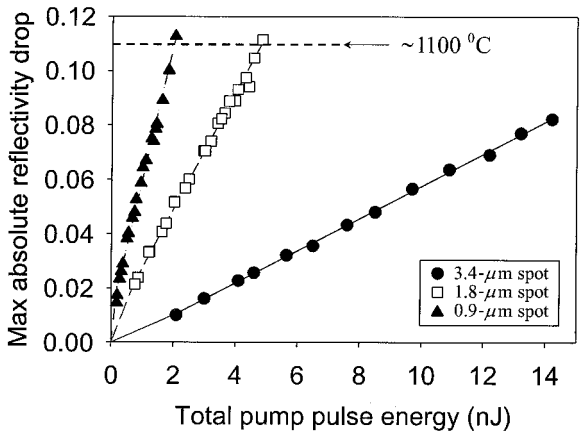

Fig. 5. Maximum absolute reflectivity drop versus total energy of the pump pulse for three different values of the focused spot size of the pump beam. The curves corresponding to the spot sizes of 0.9 and 1.8 μm are terminated at the pulse energy that causes permanent reflectivity change of the sample (burnout). According to the numerical modeling, at a slightly lower pulse energy the sample reaches the melting temperature of bulk gold in the middle of the focused spot. The curve corresponding to the spot size of 3.4 μm is terminated at the maximum pump energy available in the system; in other words, damage threshold was not reached in this case because the available pulse energy was not sufficient. The curves represent a linear fit to the experimental data points.

(solid curves). The agreement between the calculation and the experiment is reasonable. The apparent descrepancies are likely to be attributed to the inadequacy of our numerical model to account for the temperature dependence of various material parameters, as well as the complex structure of the film layers and the layer interfaces. For comparison, in Fig. 4 we show the same curves calculated with bulk values for all parameters of the system, including the thermal conductivity of the gold layer, together with the experimental data. Clearly, the agreement in this case is not as good as before, showing that our approach can be practical to estimate thermal constants of thin films that are responsible for thermal transport on a time scale slower than ~500 ps.

In the experiment, the intensity of the pump beam in all three cases with different NAs shown in Fig. 3 was adjusted so that no permanent reflectivity change resulted from any single pump pulse. The maximum absolute reflectivity drop in all three cases was close to 6%. By repeating the measurement using a different energy of the pump pulse, we found that the maximum reflectivity drop was approximately a linear function of the pump pulse energy up to the point of a permanent and unrecoverable reflectivity change. The corresponding data are shown in Fig. 5. The curves corresponding to larger NA values of the focusing lens (and higher areal energy density of the pump pulse on the sample) are terminated at the pulse energy that causes a permanent reflectivity change of the sample (burnout). The data taken at the lowest NA of the focusing lens were limited by the maximum available pump pulse energy from the laser on the sample (~14 nJ). The mechanism of burnout is unclear. However, from the thermal modeling we found that the temperature of the gold layer in the middle of the focused light beam on the sample is approximately twice as high as the spatially averaged temperature across the focused spot. Assuming that reflectivity of the gold layer is a linear function of temperature all the way to the melting point, with the proportionality constant equal to that of bulk gold at 532 nm, of the order of -2×10^{-4} 1/°C,[16] we conclude from Fig. 5 that the burnout occurs immediately (or shortly) after the gold layer in the middle of the focused light beam reaches the melting temperature of bulk gold.

B. Dynamics of Rapid Amorphization in a Quadrilayer Thin-Film Medium

As a second application example we used a quadrilayer structure as an optical data-storage medium. The sample is deposited on a 0.6-mm-thick polycarbonate substrate. Figure 6 schematically shows the cross-sectional view of the stack. It consists of a 10-nm-thick upper dielectric layer of ZnS–SiO_2, a 13-nm-thick phase-change recording layer of GeSbTeBi (GSTB), a 10-nm-thick lower dielectric layer of ZnS–SiO_2, and a 100-nm-thick silver alloy reflective layer. The latter acts both as a reflector and as a heat sink because it removes the heat from the phase-change layer.

When used as a recording medium of an optical data-storage disk, the GSTB layer is initially prepared in (or initialized to) the crystalline state. Exposure to the short focused laser pulses locally heats up the recording layer, which subsequently cools rapidly because the heat sinks into the underlying silver alloy layer. This process results in the creation of the amorphous marks on the disk and is referred to as the melt-quenched amorphization. The amorphous marks have a different reflection coefficient from the surrounding crystalline area, making it possible to read the recorded binary information by optical means. If the amorphous marks are exposed to weak

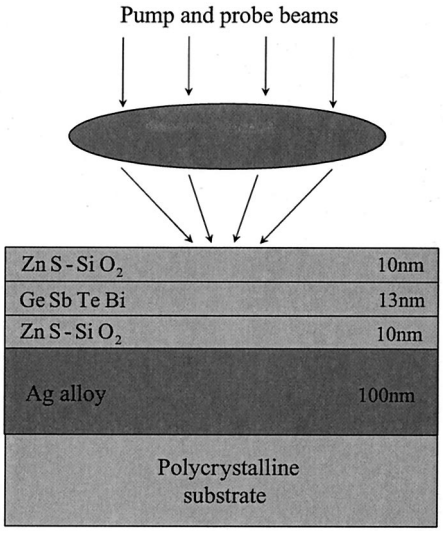

Fig. 6. Structure of the quadrilayer phase-change sample used in the experiment.

(a few milliwatts) cw laser light, they go back to their crystalline state; thus the recorded information can be erased. Typically, the melt-quenched amorphization is a much faster process than the recrystallization; the latter occurs on a time scale of tens or even hundreds of nanoseconds.

Using our system, we investigated the dynamics of melt-quenched amorphization in the precrystallized quadrilayer GSTB sample. The details of this study are reported elsewhere,[18] and this case is used here as another example illustrating the capabilities of the system. Figure 7 shows the measured reflectivity change during the crystalline-to-amorphous phase transition of the GSTB film for four different values of the pump pulse energy. The measurement setup was identical to the one used for the gold mirror characterization described above. The effective NA of the

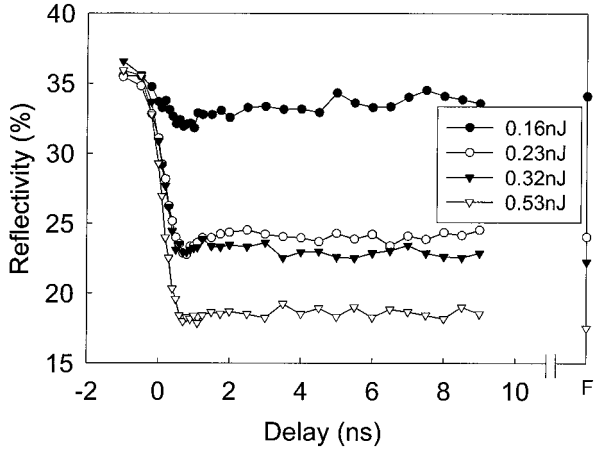

Fig. 7. Reflectivity variation during amorphization of the crystalline state of a GSTB film. Each curve corresponds to a specific value of the optical pulse energy. The rightmost data point in each curve represents the final reflectivity of the recorded mark (taken several minutes after the exposure).

focusing lens was 0.18, resulting in a spot size of 1.8 μm for the focused pump beam on the sample. In the experiment, the pump and probe beams were focused on the sample through the upper dielectric layer. Each data point in Fig. 7 represents the result of our averaging 20 independent single-shot measurements on a fresh area of the sample. After writing the amorphous marks on the sample with pump pulses, we erased them with a weak cw laser beam. If the marks turned out to be erasable, then the pump pulse energy was not high enough to cause the sample burnout. In this way we confirmed that the bottom curve in Fig. 7 (corresponding to 0.53 nJ) represents the formation of a permanent hole in the film rather than a melt-quenched amorphous mark. Marks written with a 0.16-nJ pulse are hardly distinguishable from the crystalline background when the sample is inspected with an optical microscope, even though a small mark could have been formed in the center of the focused laser beam, which is indicated by a slight drop in the reflectivity of the sample in this case (the upper curve in Fig. 7). The two middle curves in Fig. 7 represent the formation of distinguishable melt-quenched amorphous marks. In these cases, the reflectivity drops immediately after the beginning of the pulse ($t = 0.0$ ns) and reaches its lowest value at the end of the recording pulse ($t \simeq 0.6$ ns) or shortly before that. After reaching the minimum, the reflectivity slightly goes up for several hundred picoseconds before reaching its final value, which corresponds to the cooling and solidification process. Using the values of the thermal conductivity κ and the specific heat c for the GSTB film sandwiched between two dielectric layers inferred from other sources ($\kappa = 0.005$ W/cm/°C and $c = 1.5$ J/cm^3/°C), we estimate that for the duration of the pump pulse the heat diffuses into the GSTB film by ~10 nm, reaching the heat-sinking Ag alloy layer, which, due to its high thermal conductivity, rapidly dissipates the heat. Consequently, one can conclude that the melt-quenched amorphous mark forms in this sample in ≈1 ns.

In addition to the formation of the melt-quenched amorphous marks, it is interesting to note that the permanent hole is also formed in the time interval of ≈1 ns. It is likely that the hole is confined within the recording GSTB layer and is not a through hole (i.e., all the way into the plastic substrate) because there is not enough energy in the pulse to melt the fairly thick metal layer.

4. Conclusion

We have reported on a pump-and-probe thermoreflectance system with detection of individual probe pulses. The system is intended to be used for the study of phase transitions in thin films and surfaces, as well as to estimate thermal constants of such samples. By an adjustment of the focused spot size of the pump beam on the sample, the in-plane and out-of plane thermal transports can be separated and studied independently. The time resolution of the system is ~0.5 ns, and the absolute sensitivity to the ther-

mally induced reflectivity change is ~0.1%. Several design issues relevant to reduction of the measurement uncertainty have been discussed. To demonstrate the capabilities of the system, we have used it to study thermal properties of two different thin-film samples. In the case of a single-phase film sample, the numerical modeling shows reasonable agreement with the experimental data, which demonstrates that the system is sensitive enough to be used to estimate thermal constants of thin films. With a two-phase thin-film sample, the system can be used to estimate the time scale of the heat-induced phase transitions in the film.

References

1. X. Zhang, S. Chu, J. Ho, and C. Grigoropoulos, "Excimer laser ablation of thin gold films on a quartz crystal microbalance at various background pressures," Appl. Phys. A **64,** 545–552 (1997).
2. A. B. Marchant, *Optical Recording* (Addison-Wesley, Reading, Mass., 1990).
3. T. N. Thomas, C. J. Stevens, A. J. S. Choudhary, J. F. Ryan, D. Mihailovic, T. Mertelj, L. Forro, G. Wagner, and J. E. Evetts, "Photoexcited carrier relaxation and localization in $Bi_2Sr_2Ca_{1-y}Y_yCu_2O_8$ and $YBa_2Cu_3O_{7-\delta}$: a study by femtosecond time-resolved spectroscopy," Phys. Rev. B **53,** 12436–12440 (1996).
4. M. Zavrtanik, J. Demsar, B. Podobnik, D. Mihalovic, and J. Evetts, "Analysis of the photoresponse of Y-Ba-Cu-O thin films on ps to μs timescales," in *Applied Spectroscopy 1997: Proceedings of EUCAS 1977*, The Third European Conference on Applied Superconductivity, Vol. 1 of Institute of Physics Conference Series, H. Rogalla and D. H. A. Blank, eds. (Institute of Physics, London, 1997), pp. 149–156.
5. N. Taketoshi, T. Baba, and A. Ono, "Observation of heat diffusion across submicrometer metal thin films using a picosecond thermoreflectance technique," Jpn. J. Appl. Phys. **38,** L1268–L1271 (1999).
6. W. Capinski, H. Maris, T. Ruf, M. Cardona, K. Ploog, and D. Katzer, "Thermal conductivity measurements of GaAs/AlAs superlattices using a picosecond optical pump-and-probe technique," Phys. Rev. B **59,** 8105–8113 (1999).
7. G. Langer, J. Hartmann, and M. Reichling, "Thermal conductivity of thin metallic films measured by photothermal profile analysis," Rev. Sci. Instrum. **68,** 1510–1513 (1997).
8. D. Chu, M. Touzelbaev, E. Goodson, S. Babin, and R. Fabian Pease, "Thermal conductivity measurements of thin-film resist," Vac. Sci. Technol. B **19,** 2874–2877 (2001).
9. C. Paddock and G. Eesley, "Transient thermoreflectance from thin metal films," J. Appl. Phys. **60,** 285–290 (1987).
10. C. W. Siders, A. Cavalleri, K. Sokolowski-Tinten, Cs. Toth, T. Guo, M. Kammler, M. Horn von Hoegen, K. R. Wilson, D. von der Linde, and C. P. J. Barty, "Detection of nonthermal melting by ultrafast x-ray diffraction," Science **286,** 1340–1342 (1999).
11. D. Price, R. More, R. Walling, G. Guethlein, R. Shepherd, R. Stewart, and W. White, "Absorption of ultrashort laser pulses by solid targets heated rapidly to temperatures 1-1000 eV," Phys. Rev. Lett. **75,** 252–255 (1995).
12. Y. Hitoki, M. Hidetoshi, U. Ken-ichi, and R. Moore, "Ultrashort-pulse laser ellipsometric pump-probe experiments on gold targets," Phys. Rev. Lett. **91,** 075004 1–4 (2003).
13. T. Yamane, S. Katayama, and M. Todoki, "Analysis of ac temperature wave during the measurement of thermal diffusivity of two-layered platelike samples," J. Appl. Phys. **80,** 2019–2026 (1996).
14. G. Chen and P. Hui, "Thermal conductivities of evaporated gold films on silicon and glass," Appl. Phys. Lett. **74,** 2942–2944 (1999).
15. G. Palasantzas and J. De Hosson, "Mound surface roughness effects on the thermal capacitance of thin films," J. Appl. Phys. **89,** 6130–6134 (2001).
16. J. Batista, D. Takeuti, A. Mansanares, and E. da Silva, "Contrast and sensitivity enhancement in photothermal reflectance microscopy through the use of specific probing wavelengths: applications to microelectronics," Anal. Sci. **17,** S73–S75 (2001).
17. M. Mansuripur, G. Connell, and J. Goodman, "Laser-induced local heating of multilayers," Appl. Opt. **21,** 1106–1114 (1982).
18. K. Watabe, P. Polynkin, and M. Mansuripur, "Behavior of GeSbTeBi phase-change optical recording media under subnanosecond pulsed laser irradiation," Appl. Opt. **43,** 4033–4040 (2003).